

## Effects of thermal and mechanical treatments on montmorillonite homoionized with mono- and polyvalent cations: Insight into the surface and structural changes

M. Fernández<sup>a</sup>, M.D. Alba<sup>b</sup>, R.M. Torres Sánchez<sup>a,\*</sup>

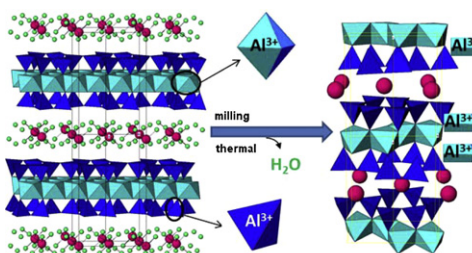
<sup>a</sup> Centro de Tecnología de Recursos Minerales y Cerámica (CETMIC-CONICET CCT-La Plata) Camino Centenario y 506, M.B. Gonnet, Argentina

<sup>b</sup> Instituto Ciencia de los Materiales de Sevilla (CSIC-US), Avda. Americo Vespucio, 49. 41092, Seville, Spain

### HIGHLIGHTS

- ▶ Total specific surface area depends of valence and size of the interlayer cation.
- ▶ Surface electrostatic interaction influences the agglomeration size of samples.
- ▶ The dehydroxylation temperature depends on the exchanged cation, with the trend:  $\text{Al} < \text{Li} < \text{Na} < \text{K} < \text{Ca}$ .
- ▶ Mechanical treatment provokes structural defects favoring the increase of the IEP values.
- ▶ The framework damage of treated  $\text{M}^{2+}$  and  $\text{M}^{3+}$ -MMT is related to the lowering of  $\text{Al}^{\text{IV}}$ .

### GRAPHICAL ABSTRACT



### ARTICLE INFO

#### Article history:

Received 16 January 2013

Accepted 22 January 2013

Available online 4 February 2013

#### Keywords:

Montmorillonite

Homoionized montmorillonite

Mechanical and thermal treatments

RMN

Zeta potential

### ABSTRACT

Smectite is a family of clay minerals that have important applications. In the majority of these clay minerals, the hydrated interlayer cations play a crucial role on the properties of the clay. Moreover, many studies have revealed that both thermal and grinding treatments affect the MMT structure and that interlayer cations play an important role in the degradation of the structure, primarily after mechanical treatment. In this study, the effects of these treatments on MMTs homoionized with mono ( $\text{Na}^+$ ,  $\text{Li}^+$  or  $\text{K}^+$ ) or polyvalent ( $\text{Ca}^{2+}$  or  $\text{Al}^{3+}$ ) cations were analyzed by the combination of a set of techniques that can reveal the difference of bulk phenomena from those produced on the surface of the particles. The thermal and mechanical (in an oscillating mill) treatments affected the framework composition and structure of the MMT, and the thermal treatment caused less drastic changes than the mechanical one. The effect of the interlayer cations is primarily due to the oxidation state and, to the size of the cations, which also influenced the disappearance of aluminum in the MMT tetrahedral sheet. These treatments caused a decrease in the surface area and an increase in the particle agglomeration and the isoelectric point. Both treatments caused the leaching of the framework aluminum. Furthermore, the mechanical treatment induced structural defects, such as the breakup of the particles, which favored the dehydroxylation and the increase of the isoelectric points of the montmorillonites.

© 2013 Elsevier B.V. All rights reserved.

### 1. Introduction

The smectite group of minerals has attracted the attention of scientists, not only because of their importance in physical, chemical and environmental processes in soils and sediments but also

\* Corresponding author. Tel.: +54 221 4840247; fax: +54 221 4710075.

E-mail addresses: [mfernandez@cetmic.unlp.edu.ar](mailto:mfernandez@cetmic.unlp.edu.ar) (M. Fernández), [alba@icmse.csic.es](mailto:alba@icmse.csic.es) (M.D. Alba), [rosats@cetmic.unlp.edu.ar](mailto:rosats@cetmic.unlp.edu.ar) (R.M. Torres Sánchez).

because of their applicability in technological, environmental and industrial processes [1–4].

Montmorillonite (MMT), which has an ideal structural formula of  $\text{Si}_4(\text{Al}_{1.67}\text{Mg}_{0.33})\text{O}_{20}(\text{OH})_4[\text{Na}_{0.33}\cdot\text{H}_2\text{O}]$ , is a smectite composed of hydrated cations sandwiched between the 2:1 (tetrahedral and octahedral) negatively charged layers.

These hydrated cations are able to modify the properties of MMT, such as its surface charge [5–6], hydroxylation capacity [7], thermal behavior [8–9], physical properties, and consequently the retention of heavy metals [10–11], dyes [12–15], herbicides [16], toxins [17–19], etc.

In 1958, Kulbicki [20] highlighted the possibility that primary exchange cations play an important role in thermal transformations of these minerals. Other changes in the behavior and properties of montmorillonite were also associated with the exchange cations, i.e., exchanged  $\text{Na}^+$  and  $\text{K}^+$ -MMT neutralized the permanent charges and reduced the temperature for the production of cristobalite [21] and the migration of different cations into the MMT structure after thermal treatment caused a reduction in the swelling and adsorption capacity and increased the mean particle diameter [22,8]. Due to the improvement of their surface structures with respect to raw MMT, exchanging the cations in montmorillonites with  $\text{Al}^{3+}$ ,  $\text{Cu}^{2+}$ , etc. allowed them to be used as adsorption catalysts [23–28]. In addition, studies have been performed to obtain exchanged clay for industrial uses as alternative coatings for brittle-matrix fibers [29].

In previous works, [5–6,30] it was shown that both thermal and grinding treatments affect the MMT structure and that interlayer cations play an important role in the degradation of the structure, primarily after mechanical treatments. Specifically, the analysis of X-ray diffraction patterns of MMT exchanged with different cations revealed different shifts of the  $d(001)$  interlayer spacing as a consequence of the water molecules associated with each of the cations [31–32]. The thermal treatment changed the interlayer spacing of homoionized MMT to approximately 0.93 nm, and the mechanical treatment destroyed the lamellar packing to a greater extent for the mono- than for the polyvalent exchanged cations, due to a greater electrostatic attraction of the latter to the surface of MMT. Moreover, the values of the isoelectric point (IEP), which were obtained through measurements of the diffusion potential, indicate that the damaged structure produced by the mechanical treatment of  $\text{Na}^+$ ,  $\text{Li}^+$ , and  $\text{K}^+$  and the thermal treatment of  $\text{Ca}^{2+}$  exchanged MMT samples causes a surface charge behavior similar to that of an oxide mixture with an equivalent composition [33]. The IEP of homoionic-exchanged MMTs with different interlayer cations [6] exhibited a similar behavior to those obtained using the coagulation method [23].

The greater IEP pH values obtained for thermally treated MMT exchanged with  $\text{Na}^+$ ,  $\text{Li}^+$ , and  $\text{K}^+$  than for those exchanged with  $\text{Ca}^{2+}$  and  $\text{Al}^{3+}$  and also for all the mechanical treated samples was attributed to the greater amounts of Al released from the structure, which produces a greater Al coating of the MMT surface [5].

Previous studies performed on thermal or mechanically treated kaolin indicated an enhancement of the reactivity for zeolite synthesis, which was attributed to a better extraction of Al and Si ions from the collapsed structure that originated in the Al (IV) to (VI) modification, as revealed by XPS analysis [34–35].

The purpose of this study is to determine the effect of thermal or mechanical treatments on the structure of MMT homoionized with mono- and polyvalent cations through the combination of total specific surface and apparent diameter (Dapp), Zeta potential curves, differential thermal analysis and single-pulse (SP) MAS-NMR measurements. The employed techniques can reveal the difference between the bulk phenomena from those produced on the surfaces of the particles.

**Table 1**  
Chemical analysis of the  $V_0$  sample.

SiO <sub>2</sub>	Al <sub>2</sub> O <sub>3</sub>	Fe <sub>2</sub> O <sub>3</sub>	MgO	CaO	Na <sub>2</sub> O	K <sub>2</sub> O	Li <sub>2</sub> O	H <sub>2</sub> O
59.09	19.63	3.65	2.30	1.21	2.14	0.48	<0.01	10.62

## 2. Materials and methods

The raw smectite sample (from Volclay, Wyoming, USA) named  $V_0$  contains 95% montmorillonite with quartz and feldspar as impurities and a cationic exchange capacity (CEC) of 63.5 meq/100 g. The results of the chemical analysis [5] of the purified montmorillonite sample are presented in Table 1.

The homoionized montmorillonites (named  $V_{\text{Na}}$ ,  $V_{\text{Li}}$ ,  $V_{\text{K}}$ ,  $V_{\text{Ca}}$  and  $V_{\text{Al}}$ ) were obtained by three consecutive treatments with 2 N aqueous chloride solutions of the respective cations. The excess salt was removed by several washings with distilled water following by centrifuging (15,000 rpm) until the filtrate was free of  $\text{Cl}^-$  ( $\text{AgNO}_3$  test).

These samples were mechanically treated in an oscillating mill (Herzog HSM 100) with a rotational frequency of 12.5 Hz for 300 s. The resulting materials will be referenced in this work using subscripts that represent the cation followed by the grinding time ( $V_{\text{Li}300\text{s}}$ ,  $V_{\text{Ca}300\text{s}}$ , etc.). The thermal treatments consisted of calcining the samples in air at 600 °C for 1 h, and the products were named as follows:  $V_{\text{K}600\text{C}}$ ,  $V_{\text{Ca}600\text{C}}$ , etc.

The external specific surface area (ESSA) was determined by nitrogen adsorption at 77 K (SN2) using a Micromeritics model Gemini V, and all samples were dried at 100 °C for 12 h under high vacuum before the nitrogen sorption measurements.

The total specific surface area (TSSA) was determined from the adsorption of water vapor at a relative humidity of 0.56, as described elsewhere [36].

The apparent equivalent sphere diameter (Dapp) was obtained by dynamic light scattering (DLS) measurements using a Brookhaven 90Plus/Bi-MAS with the Multi Angle Particle Sizing Option, which was operated at  $\lambda = 635$  nm with a 15 mW solid state laser, scattering angle of 90°, and a temperature of  $25 \pm 0.1$  °C. All sample suspensions (1% w/w) were prepared using water with  $10^{-2}$  M  $\text{MCl}_x$  ( $M = \text{Na}, \text{Li}, \text{K}, \text{Ca}$  or  $\text{Al}$ ) or with  $10^{-3}$  M KCl solutions and sonicated for 5 min, and then the particle size determinations were conducted.

Electrokinetic potentials were determined in same Brookhaven equipment (electrophoretic mobility function) utilized for Dapp measurement. The electrophoretic mobility was converted into zeta potential values using the Smoluchowski equation. For each determination, 0.05 g of sample was dispersed in 100 mL of a  $10^{-3}$  M KCl solution, and the slurry was stirred. To generate zeta potential versus pH curves, the pH of the slurry was adjusted using dilute HCl and KOH solutions followed by magnetic stirring until equilibrium was attained (10 min).

TG/DTA experiments were conducted using a NETZSCH STA 409 PC/PG with alumina as a reference. The samples were placed in Pt crucibles and maintained under an air atmosphere throughout the heating period. The temperature was increased at a constant rate of 10 °C/min.

Single-pulse (SP) MAS-NMR experiments were performed using a Bruker DRX400 spectrometer equipped with a multinuclear probe. Powdered samples were packed in 4 mm zirconia rotors and spun at 10 kHz.  $^{29}\text{Si}$  MAS NMR spectra were acquired at a frequency of 79.49 MHz using a pulse width of 2.7  $\mu\text{s}$  ( $\pi/2$  pulse length = 7.1  $\mu\text{s}$ ) and a delay time of 3 s.  $^{27}\text{Al}$  MAS-NMR spectra were recorded at 104.26 MHz with a pulse width of 0.92  $\mu\text{s}$  ( $\pi/2$  pulse length = 9.25  $\mu\text{s}$ ) and a delay time of 0.1 s. The chemical shift values are reported in ppm from tetramethylsilane for  $^{29}\text{Si}$  and from 0.1 M  $\text{AlCl}_3$  solution for  $^{27}\text{Al}$ .

### 3. Results

#### 3.1. Apparent diameter and total specific surface area

From the chemical composition (Table 1) and following the procedure proposed by Siguin et al. [37], the structural formula of the raw montmorillonite was determined to be  $[\text{Si}_{43.99} \text{Al}_{0.01}] (\text{Al}_{1.58} \text{Fe}^{3+}_{0.186} \text{Mg}_{0.233} \text{O}_{20} (\text{OH})_2 \text{M}^{+}_{0.233} \cdot \text{H}_2\text{O})$ .

The structural formula indicated a low charge montmorillonite ( $\text{M}^{+}_{0.233}$ ), and a substitution of octahedral Al with 9.3% Fe and 11.65% Mg was observed. The amount of Mg allowed the sample to be classified as Cheto-type (1.38% MgO), in which the high iron content would modify the Cheto-type montmorillonite behavior [38].

An accurate determination of the specific surface area (SSA) of swelling clay minerals, such as montmorillonite, is not straightforward using nitrogen. Specific interactions generated between the probe molecule and the polar surface sites indicate that nitrogen is not the best probe molecule to use for this purpose [39]; therefore, the use of nitrogen only allows the external specific surface area (ESSA) of the clay to be determined [40–41], which can range between 5 and 10% of the total specific surface area (TSSA) depending on the particle size and primarily on the amount of stacked sheets that form the tactoids [42].

The water molecules penetrate the interlayer space, and the TSSA value resulting from its adsorption included the inner surface and allowed the TSSA to be determined. Because water adsorption induces swelling of the clay, TSSA determination by water adsorption may be used with the precaution of similar initial outgassing conditions, the use of a relative humidity >54% and considering that the residual water content strongly depends on the nature of the cation [39,43,44]. The TSSA and ESSA of the homoionized and treated samples are summarized in Table 2.

For smectite clays in general, thermal treatments produce a decrease in the ESSA value [45–46], whereas mechanical treatments generate an increase in this value [45,47]. Because natural smectites generally have a high content of Na, the  $V_{\text{Na}}$  sample followed the previously mentioned assumption for the ESSA values obtained after each treatment (Table 2). The presence of different exchangeable cations strongly modifies the ESSA value and pore volumes for the dried montmorillonite samples ([39] and references therein) without following a unique behavior with thermal or mechanical treatments.

The TSSA values obtained (Table 2) for the homoionized samples are consistent with those deduced from the unit cell parameters [39–40], and particularly that of the  $V_{\text{Na}}$  sample was similar to the values obtained with a similar method from Argentine MMT samples with a high Na content and a Wyoming MMT sample [18,40].

The lower TSSA value of the  $V_{\text{K}}$  sample among the monovalent interlayer cations would be explained by the striking stability of the single layer hydrate, which inhibits further swelling of the clay [48–49] in contrast to  $\text{Li}^+$ , which tends to hydrate [49] and produce a TSSA value that is 20 % greater than that for the  $V_{\text{K}}$  sample.

The higher TSSA values obtained for the  $V_{\text{Al}}$  and  $V_{\text{Ca}}$  samples with respect to monovalent interlayer cations can be due to their

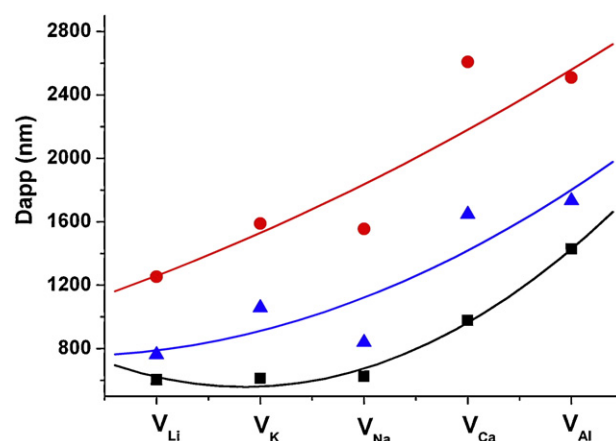


Fig. 1. Dapp values of indicated samples in: (■) aqueous and ionic strength suspensions (▲)  $10^{-2}$  M MCl (chloride of the respective cations) and (●)  $10^{-3}$  M KCl.

capacity to form up to three interlayer sheets of water [50]. However, primarily compared to the  $V_{\text{Na}}$  sample, the  $V_{\text{Al}}$  and  $V_{\text{Ca}}$  samples have a slower swelling capacity that is generated by the greater interplatelet attraction produced by the polyvalent cations [51–52].

The thermal treatment of all samples generated approximately a 90% decrease of the initial TSSA values depending on the exchanged cations [53] and changes in the porosity system [43]. Chorom and Rengasamy [8] attributed this behavior to different bonding characteristics and migration between small (Li and Al with ionic radii <0.7 Å) and large (Na, Ca and K) cations after thermal treatment (up to 400°C) and the observed swelling and dispersion capacity behavior.

The similar TSSA values obtained for the thermally treated  $V_{\text{Li}}$  and  $V_{\text{Al}}$  samples can be attributed to the migration of the respective cations to hexagonal cavities with a layer charge reduction [7] and consequently the surface area hydration capacity [40]. For the  $V_{\text{Na}}$ ,  $V_{\text{K}}$  and  $V_{\text{Ca}}$  samples, the thermal treatment reduced their hydration [8] and consequently their TSSA values.

Mechanical treatment produced a ca. 50% decrease of the TSSA values, which was primarily due to greater structural damage [54] than that produced by thermal treatment. A high correlation value ( $R^2 = 0.99$ ) between the TSSA values for the thermally and mechanically treated samples was observed without considering the  $V_{\text{Al}}$  sample. The lower structural damage of  $V_{\text{Al}}$  after both treatments among all the samples studied ( $V_{\text{Al}} < V_{\text{Ca}} < V_{\text{K}} < V_{\text{Li}} < V_{\text{Na}}$ ; [5]) could be partially responsible for its different decrease in the TSSA value, which was primarily attributed to the migration of Al to hexagonal cavities and to different electrostatic bonds with respect to that of Li [8].

The particle size aggregation was followed by Dapp measurements in an aqueous suspension and in suspensions with ionic strength ( $10^{-2}$  MCl and  $10^{-3}$  M KCl) (Fig. 1).

In a water suspension, a decrease in the agglomerate size was observed for the homoionized samples that followed the order of

Table 2  
External (ESSA) and total (TSSA) specific surface areas of indicated samples.

Sample	Raw ( $\text{m}^2 \text{g}^{-1}$ )		Mechanically treated ( $\text{m}^2 \text{g}^{-1}$ )		Thermally treated ( $\text{m}^2 \text{g}^{-1}$ )	
	TSSA	ESSA	TSSA	ESSA	TSSA	SN <sub>2</sub>
$V_{\text{Na}}$	855 ± 20	38.78 ± 2.02	301 ± 11	45.23 ± 2.31	66 ± 5	15.34 ± 1.65
$V_{\text{K}}$	508 ± 15	16.42 ± 1.62	206 ± 10	22.27 ± 1.02	44 ± 3	22.85 ± 1.50
$V_{\text{Li}}$	637 ± 17	32.14 ± 2.13	299 ± 12	27.38 ± 1.78	61 ± 6	23.89 ± 0.87
$V_{\text{Ca}}$	757 ± 19	14.15 ± 1.61	504 ± 14	29.95 ± 1.27	105 ± 8	16.32 ± 2.01
$V_{\text{Al}}$	959 ± 24	13.04 ± 0.98	454 ± 14	36.63 ± 1.82	51 ± 4	23.03 ± 2.43

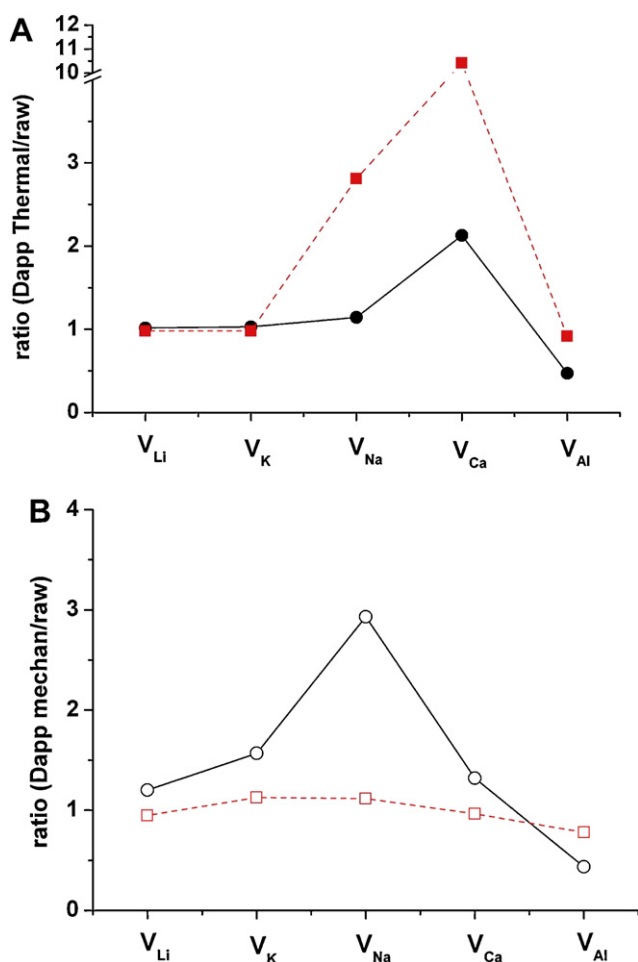


Fig. 2. Ratio of (A) Dapp thermal/raw and (B) mechanical/raw samples. Red dashed lines and (■, □) correspond to ionic strength =  $10^{-2}$  M (Chloride of the respective cations) and black solid lines and (●, ○) correspond to the aqueous suspension.

$V_{Al} > V_{Ca} > V_{Na} \approx V_{Li} \approx V_{K}$ , which was related to the increase from mono to polyvalent cations and consequently to a stronger chemical binding from the cation to the surface of the MMT.

In presence of  $10^{-2}$  M MCl (M = the same cation exchanged), the obtained Dapp values were higher and followed a similar order to that observed in the aqueous suspension. The higher Dapp values observed in presence of ionic strength solutions indicated the influence of surface electrostatic interactions generated by the exchanged cations, as in the aqueous suspension, and double layer thickness compression generated by the different valences of the utilized cations.

The presence of  $10^{-3}$  M KCl must generate an electric double layer compression less than  $10^{-2}$  M and consequently an increase of the Dapp values. However, a greater increase of the Dapp values was obtained in  $10^{-3}$  M KCl for all the samples and was attributed to the exchange of each interlayer cation for  $K^+$  coming from the solution. Considering that  $10^{-3}$  M is a two-order of magnitude greater concentration than that obtained from considering the amount of cations that can be exchanged (CEC 63.5 meq/100 g), the exchange with  $K^+$  from the solution can be produced by modifying the electric double layer compression.

Thermal treatment of the samples generated increased Dapp values (Fig. 2) for the respective raw MMTs that are consistent with results reported by Chorom and Rengasamy [8], with the exception of the V<sub>Al</sub> sample, in which a similar behavior could be assigned as that observed for the TSSA values.

A linear trend between the Dapp and TSSA values was observed for the raw samples, which improved for the thermally treated samples and even worsened for the mechanically treated samples, which was related to the meso- and micro-porous changes associated with both treatments [44,54].

In the aqueous suspension, the influence of surface electrostatic interactions on the agglomeration behavior was evidenced by graphing (not shown) the correlation between the Dapp and IEP values (determined elsewhere, [5]). For the raw homoionized samples, a linear trend for the Dapp (obtained in aqueous suspension or  $10^{-3}$  M KCl) and IEP values was observed, and the linear trend improved when the Dapp values in chlorides of the respective cation suspensions were considered.

Similarly, the linear correlation of the values of mean particle diameter and zeta potential, which were measured elsewhere [8] without ionic strength control and at different pH values (range 4.87–6.47) for a Wyoming MMT (CEC = 80 meq/100 g), yielded a  $R^2 = 0.92$ .

In aqueous or in ionic strength ( $10^{-2}$  M) suspensions, the Dapp values of the thermally and mechanically treated samples revealed different agglomeration behavior than those obtained for the raw homoionized samples. For a better comparison of the Dapp values among samples and treatments in both suspensions, the relationship between thermal/raw and mechanical/raw samples in aqueous and ionic strength ( $10^{-2}$  M chloride of the respective cations) suspension is presented in Fig. 2A and B.

For the thermally and mechanically treated samples, Dapp correlations with TSSA cannot be considered due to the leaching of octahedral Al after both treatments (up to 16.9 mg/g clay, [43]) and different behavior of the aluminum with the remnant MMT surface, formation of hydroxoaluminum species [5], the enrichment of aluminum ions at the edges and/or to the face (+) edge (-) contacts [44], and/or the migration of Al cations from the original trans-octahedral sites to formerly unoccupied five-fold prisms [55].

As previously indicated for the raw samples, the effects that influence the size of the agglomerates in the treated samples include the valence of the exchanged cation, which modifies the external surface electric charge (interlayer does not change its charge [56]), the valence of the cation used to maintain the ionic strength of the suspension, which compresses the electrical double layer as function of its valence ( $Li < Ca < Al$ ) and the different leachings of octahedral Al after each treatment (from 0.02 to 0.06 and from 0.01 to 0.03 mg/g for monovalent mechanically and thermally treated samples, and from 0.002 to 0.006 mg/g and from 0.021 to 0.024 mg/g for polyvalent mechanically and thermally treated samples), which modifies the IEP.

The relationships between the size of agglomerates in the thermal/raw or mechanical/raw samples in ionic strength and water suspensions follow a similar shape, which indicates the influence of the valence of the cation-exchanged that modifies the external surface electric charge.

The size of the agglomerates in the thermal/raw samples was greater in the ionic strength suspension ( $10^{-2}$  M) than in water suspensions, whereas the opposite behavior was observed for the size of agglomerates in the mechanical/raw samples. This result must indicate both the influence of ionic strength and the different releases of structural Al after each treatment.

Fig. 3 presents the IEP obtained for the same samples and treatments determined by the diffusion potential in  $10^{-3}$  M KCl extracted from [5].

Fig. 3 revealed higher pH values for the IEP obtained by the greater amount of structural Al released generated for monovalent respect to bi- or tri-valent cations exchanged MMTs in presence of a  $10^{-3}$  M KCl suspension, which generated the same double layer compression for all samples. The slight difference in the IEP values

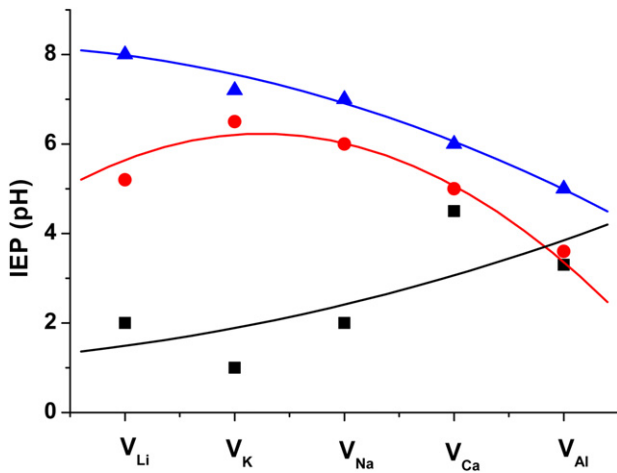


Fig. 3. IEP for (■) raw; (●) thermal and (▲) mechanical treated samples (data extracted from [5]).

for the V<sub>Al</sub> and V<sub>Ca</sub> samples was attributed to a reinforcement of the clay structure to a greater extent than monovalent cations against mechanical or thermal treatments [5].

### 3.2. Zeta potential curves

The two different types of charges (permanent negative charge on the face and the charge of the edge changing from negative to positive with decreasing pH) of the montmorillonite surface determine the zeta potential. The predominance of the negative charges on the faces of the particles compared to the positive charge on the

edges generates a negative net charge in all the investigated pH values [56], as shown in Fig. 4A.

For the V<sub>Na</sub>, V<sub>Li</sub> and V<sub>K</sub> samples, the zeta potential values (approximately -20 mV) exhibit flat curves without significant changes over a wide range of pH values (from pH 2–8), which is similar to previous reports [45,57–59].

The zeta potential curves (Fig. 4A) indicate some ordering among the homoionized samples and decreasing of the zeta potential by higher double layer compression from di- an trivalent respect to monovalent cations [60]: V<sub>Al</sub> ≈ V<sub>Ca</sub> > V<sub>Li</sub> ≈ V<sub>K</sub> > V<sub>Na</sub>, but a zero potential cannot be observed for any of the investigated samples. The use of the potential diffusion method allowed determination of the isoelectric point (IEP) of the same samples (Fig. 3), whose ordering among the samples follows a similar order to that observed in Fig. 4A.

The thermally treated samples (Fig. 4B) exhibited an increase of the negative zeta potential with respect to the raw homoionized samples, which is consistent with that observed by Thomas et al. [57] for low layer charge montmorillonite. Among the thermally treated samples, the di- and trivalent samples strongly decreased the negative zeta potential with respect to their corresponding raw homoionized samples; however, for the monovalent thermally treated samples, only the V<sub>Na</sub> sample exhibited a strong increase of the negative zeta potential with respect to the raw homoionized sample.

The mechanically treated di- and trivalent samples (Fig. 4C) exhibited a similar increase of the negative zeta potential with respect to the raw homoionized samples as that observed for the thermally treated samples, whereas the mechanically treated monovalent samples exhibited a significant increase in the negative zeta potential compared to the respective raw homoionized samples.

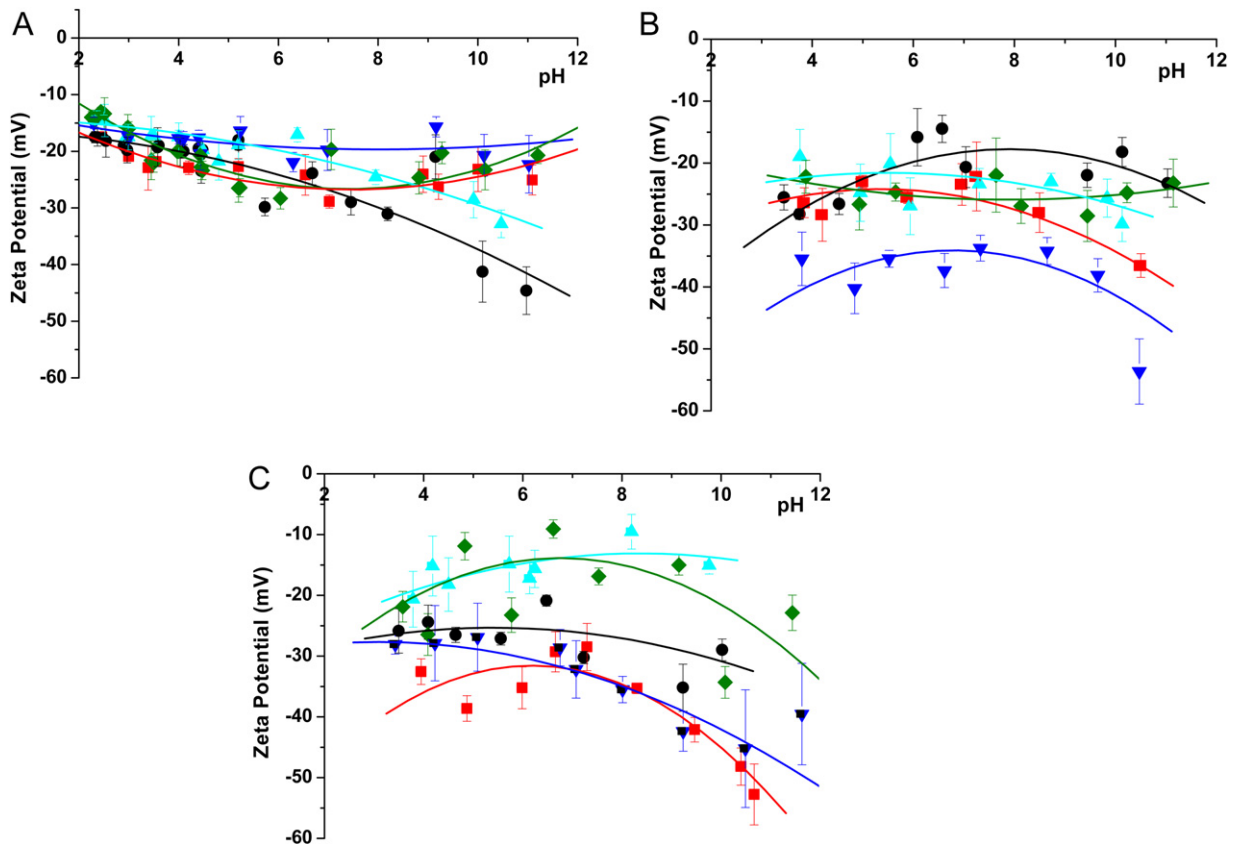


Fig. 4. Zeta potential curves (A) raw; (B) thermally treated and (C) Mechanically treated samples. Symbols indicate: (▲) V<sub>Al</sub>; (●) V<sub>Ca</sub>; (◆) V<sub>K</sub>; (■) V<sub>Li</sub> and (▼) V<sub>Na</sub> samples.

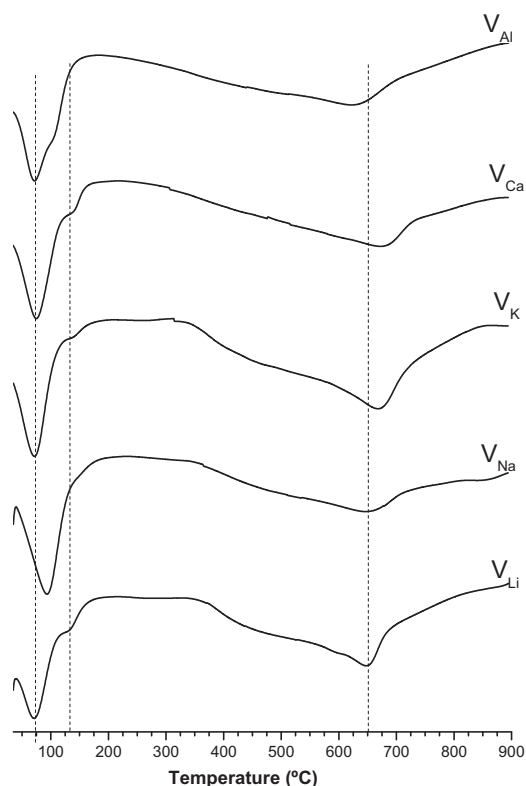


Fig. 5. DTA curves of the raw samples.

Sondi and Pravdic [45] indicated that the breakup of the particles by milling creates new edge planes without changing the character of the basal planes and influences the adsorption of ions and other charged species. These new edge planes and the octahedral aluminum loss by mechanical treatment had been reported to contribute to the increase of the IEP (Fig. 3) [43] and consequently to the observed decrease of the negative zeta potential of the treated samples.

### 3.3. Thermal analysis

Thermal analyses of the raw and treated samples were conducted to analyze the dehydration and dehydroxylation processes. Fig. 5 presents the DTA curves obtained from the raw MMTs from room temperature to 950 °C. The primary process observed from the products corresponds to several endothermic peaks that may reflect water molecules with different bonded strengths to the structure accompanied by a weight loss at temperatures below 250 °C. This process can be ascribed to the dehydration of the external surface and of the interlayer space of the montmorillonites. From this temperature, the samples exhibit a loss of weight accompanied by several endothermic peaks, which are most likely due to the dehydration of hydroxyl groups, and accumulative weight loss values at 900 °C being ca. 5%. The dehydroxylation

Table 4  
Weight losses for the raw and after thermal or mechanical treatment of the samples.

Sample	Raw		Mechanical treatment		Thermal treatment	
	250–500 (°C)	500–900 (°C)	250–500 (°C)	500–900 (°C)	250–500 (°C)	500–900 (°C)
V <sub>Li</sub>	1.1	4.2	2.9	1.9	0.4	3.2
V <sub>Na</sub>	0.9	3.2	3.6	2.3	0.8	2.8
V <sub>K</sub>	0.7	4.2	2.0	2.7	0.5	3.0
V <sub>Ca</sub>	0.9	3.8	2.7	2.5	0.9	2.0
V <sub>Al</sub>	1.6	3.5	2.9	2.5	1.2	1.5

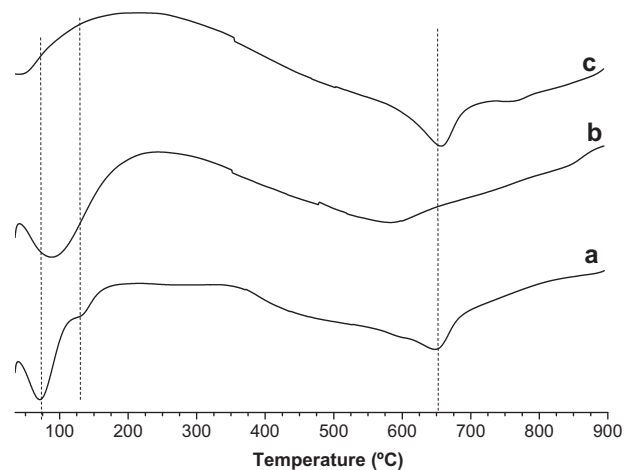


Fig. 6. DTA curves of the a) V<sub>Li</sub>, b) V<sub>Li 300s</sub> and, c) V<sub>Li 600c</sub> samples.

Table 3  
Weight losses for the dehydration process between 25 °C and 250 °C.

Sample	Loss weight (%)	Water (mol/cation)	$\Delta H^{\circ}_{\text{hyd}}$ (kJ/mol)
V <sub>Li</sub>	11.5	16.3	–515
V <sub>Na</sub>	9.9	13.9	–405
V <sub>K</sub>	7.2	9.9	–321
V <sub>Ca</sub>	13.3	38.7	–1592
V <sub>Al</sub>	13.7	59.8	–4660

temperature depends on the cation nature and follows the sequence Al < Li < Na < K < Ca. Smaller interlayer cations favor the dehydroxylation, which was observed by the decreasing of the dehydroxylation temperature. With the exception of Ca, the dehydroxylation process was favored when the surface area increased.

Fig. 6 presents the DTA curves of the V<sub>Li</sub> sample and those of the sample after the mechanical and thermal treatments; similar curves are observed for the remainder of the samples. No endothermic peak in the dehydration process is observed after the thermal treatment; however, the dehydration of the sample occurs at a higher temperature after the mechanical treatment. Regarding the dehydroxylation process, the temperature decreases after the mechanical treatment and the loss weight increases in the lower temperature range with respect to the higher temperature range (Table 4). This behavior cannot be explained by the observed decrease of the surface area after the treatment but can be explained by considering, as previously reported for the IEP values, that the mechanical treatment provokes the breakup of the particles by milling, which creates new edge planes that favored the dehydroxylation of the samples. No change is observed in the dehydroxylation temperature after the thermal treatment, although the loss weight decreases between 12% for V<sub>Na</sub> and 50% for V<sub>Al</sub>.

Table 3 summarizes the weight loss that occurred during the dehydration processes, and the amount of water molecules per cation increases as the hydration enthalpy becomes more negative. The number of water molecules per cation is directly correlated to

the hydration enthalpy of those cations in aqueous solution and is consistent with the low influence of the electrostatic field on the interlayer space in low charged montmorillonites. Table 4 presents the weight loss for the raw samples and the samples after thermal or mechanical treatment.

### 3.4. NMR measurements

The  $^{29}\text{Si}$  MAS NMR spectra of the MMTs homoionized with different cations (Fig. 6 left) are characterized by two sets of signals. One signal is at ca.  $-108$  ppm, which was attributed to silicon atoms in the three-dimensional silica network ( $Q^4$  state) [61], and it is consistent with the presence of quartz as an impurity [30,62]. The other broad signal is in the range between  $-105$  and  $-80$  ppm and it is the convolution of three overlapped signals (Supplementary Tables 6–10). The signal at ca.  $-100$  ppm is due to a feldspar impurity [30], and the two other signals at ca.  $-94$  ppm and ca.  $-87$  ppm were attributed to silicon atoms in the  $Q^3$  (OAl) and  $Q^3$  (1Al) environments of MMT, respectively [63–64]. When the interlayer sodium is replaced by the other cations, the  $^{29}\text{Si}$  MAS NMR spectra exhibit similar features, but the  $Q^3$  (mAl) signals shift towards lower frequencies. Weiss et al. [65] observed that the dioctahedral micas with similar tetrahedral Al substitution and overall layer charge have slightly different  $^{29}\text{Si}$  chemical shifts (up to 1.6 ppm) for their  $Q^3$  (OAl) sites. This behavior was explained on the basis of tetrahedral rotation ( $\alpha$ ) within the crystallographic a–b plane, which is caused by differences in the radii of the interlayer cations.

The  $^{27}\text{Al}$  MAS NMR spectra (Fig. 7right) exhibit a large peak at ca. 0 ppm, which indicates that a considerable amount of the aluminum is in the octahedral Al environments and is consistent with the octahedral character of the MMT [66–68]. Additionally, two poorly resolved peaks at ca. 58 and 67 ppm were attributed to four-coordinate tetrahedral aluminum [66,69]. The shoulder at ca. 67 ppm corresponds to a small amount of tetrahedral aluminum in

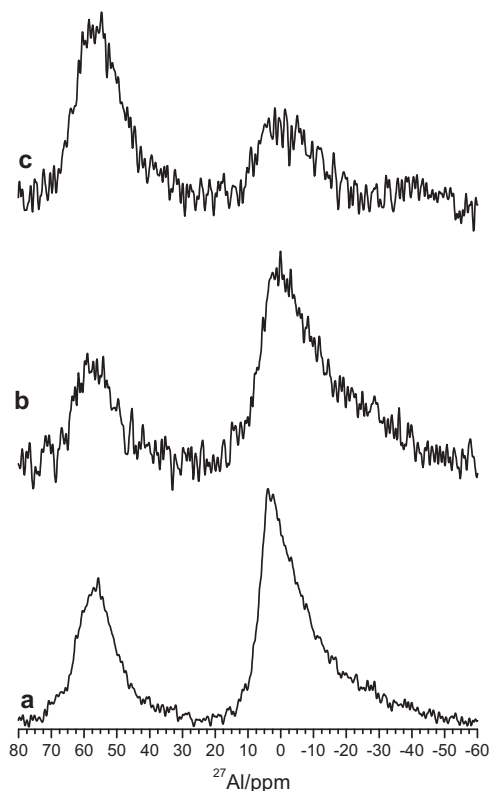


Fig. 8.  $^{27}\text{Al}$  MAS NMR spectra of: a)  $V_{\text{Na}}$ , b)  $V_{\text{Na600C}}$ , and, c)  $V_{\text{Na300S}}$  samples.

the MMT, and the peak at ca. 58 ppm corresponds to aluminum in the impurity phase of feldspar [66].

The thermal and mechanical treatments caused important changes at short-order range. Tables 5–9 (Supplementary

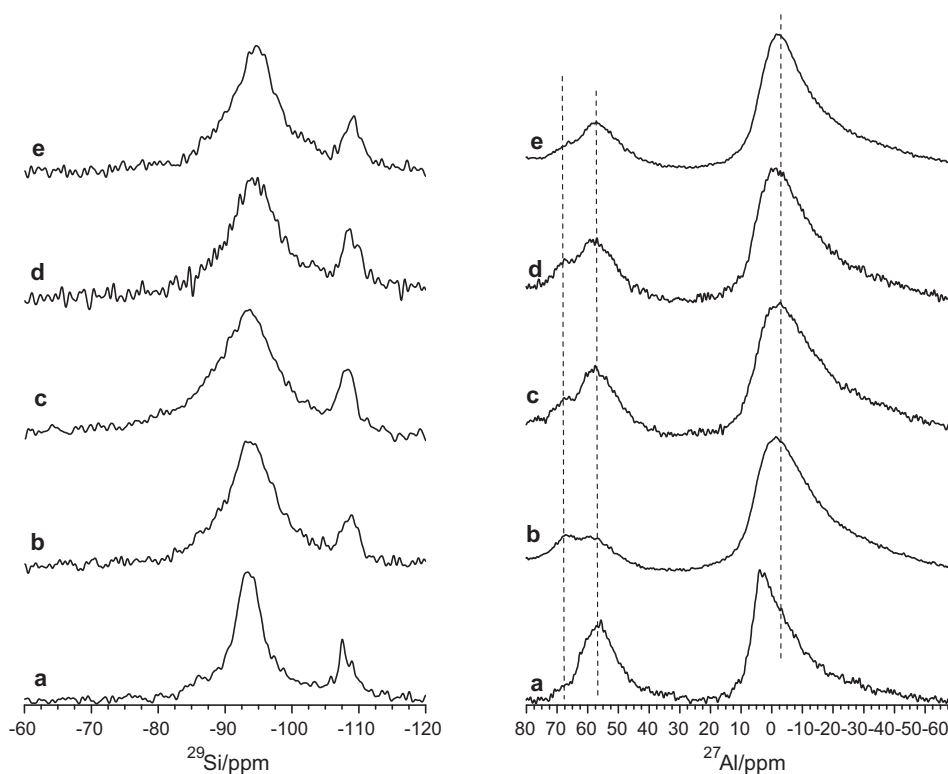


Fig. 7.  $^{29}\text{Si}$  and  $^{27}\text{Al}$  MAS NMR of the a)  $V_{\text{Na}}$ , b)  $V_{\text{Li}}$ , c)  $V_{\text{K}}$ , d)  $V_{\text{Ca}}$ , and, e)  $V_{\text{Al}}$  samples.

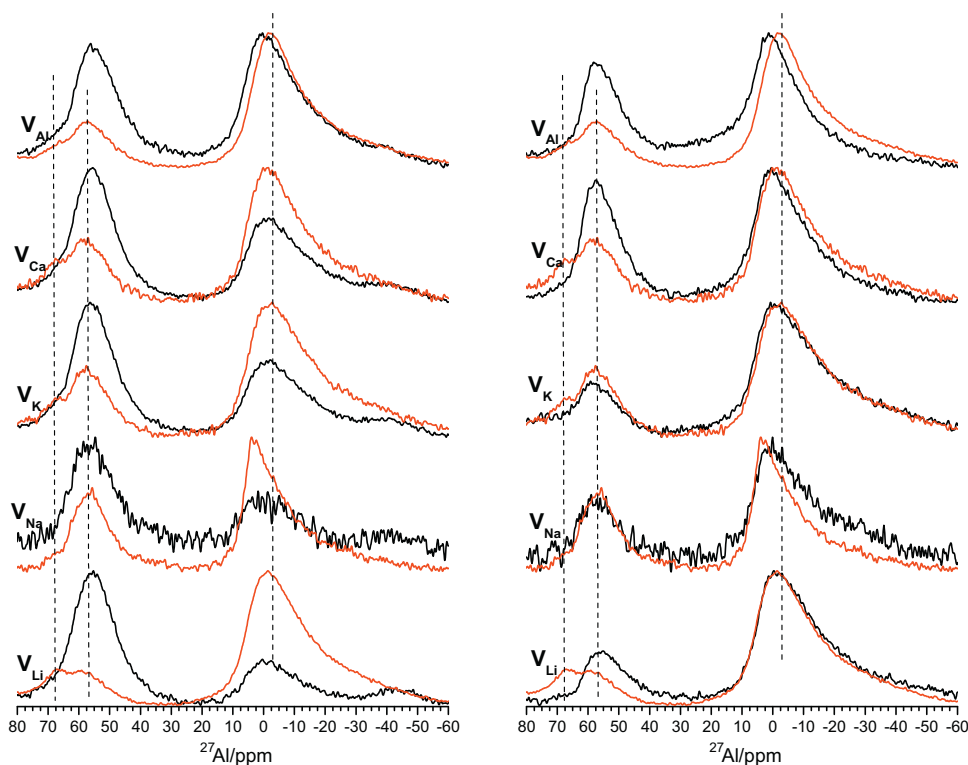


Fig. 9.  $^{27}\text{Al}$  MAS NMR spectra of montmorillonite Volclay: raw (red) mechanically treated (left, black) and heated at  $600^\circ\text{C}$  (right, black).

Material) summarized the contribution of the Si sites to the  $^{29}\text{Si}$  MAS NMR spectra. In general, the thermal treatment caused a small shift of the  $\text{Q}^3$  (0Al) peak and the disappearance of the  $\text{Q}^3$  (1Al) environment. Similar changes were observed by Dékány et al. [70] during acid treatment of sepiolite, which provoked its dealumination. These changes were more evident after the mechanical treatment, in which an increase of the peak at  $-100$  ppm parallel to a decrease of the  $\text{Q}^3$  (0Al) Si environment was observed. No clear relationship between the thermal changes and interlayer cations was observed, but, the interlayer cations influenced the short-order changes after the mechanical treatment. Specifically, the contribution of the Si site at  $-100$  ppm is inversely proportional to the total weight loss in the temperature range of  $250$ – $900^\circ\text{C}$  measured by TG; the only exception was Li. The loss of interlayer water after the thermal treatment (see TG results) produces a broadening of the Si  $\text{Q}^3$  (0Al) peak.

Considerable rearrangement of the octahedral layer of the  $\text{V}_{\text{Na}}$  sample was observed upon dehydroxylation of the structure (Fig. 7). The  $^{27}\text{Al}$  MAS NMR spectrum of the untreated  $\text{V}_{\text{Na}}$  sample (Fig. 7 left) contains a prominent peak at ca.  $0$  ppm, which indicates that most of the detectable aluminum atoms are in octahedral sites. Upon heating the  $\text{V}_{\text{Na}}$  sample at  $600^\circ\text{C}$ , no changes in the octahedral signal were observed, but the mechanical treatment provoked a drastic decrease of the  $^{27}\text{Al}$  octahedral signal without observable 5-coordinated aluminum that was most likely due to the formation of a quite distorted coordination sphere, which causes a high quadrupolar broadening. Both treatments caused the disappearance of the signal at ca.  $67$  ppm that corresponds to aluminum in the MMT tetrahedral sheet, which is consistent with the observed disappearance of the  $^{29}\text{Si}$   $\text{Q}^3$  (1Al) site (Table 5). These changes are also evident in the  $^{27}\text{Al}$  MAS NMR spectra of the MMT intercalated with the other alkali cations, including Li and K (Fig. 8), and the only difference is that the decrease of octahedral Al after mechanical treatment follows the order of  $\text{Li} > \text{Na} > \text{K} > \text{Ca} > \text{Al}$  (Fig. 9left). For cations with an oxidation state equal to  $+1$ , smaller interlayer

cations favor the dehydroxylation process, as was observed by the dehydroxylation temperature (see DTA results), which causes a decrease of the six-coordinated aluminum. The  $\text{V}_{\text{Ca}}$  and  $\text{V}_{\text{Al}}$  samples exhibit less drastic changes on octahedral Al after the mechanical treatment; these changes decrease as the oxidation state of the cation increases (Fig. 9left). The trend in the decrease of the aluminum coordination is in good agreement with the increase in the Dapp value, which the  $\text{V}_{\text{Li}}$  sample being an exception.

After the thermal treatment, the decrease in the octahedrally coordinated aluminum is less noticeable (Fig. 9right) and it does not have a direct implication in the changes of the Dapp values.

The NMR data revealed the presence of tetra-, penta-, and octahedrally coordinated Al forms in the mechanically treated samples and only tetra- and octahedrally coordinated Al in the  $500$  and  $900^\circ\text{C}$  kaolinite transformation, respectively [34].

#### 4. Conclusions

In general, a structural and compositional effect on MMT is observed after a thermal or mechanical treatment. The latter treatment produces a major effect, which depends on the nature of the interlayer cation. The effect of the interlayer cations is mainly due to their oxidation state and, to a lesser extent, the size of the cations.

As expected, a quasi-linear correlation was observed between the surface area and the agglomeration of the particles. Both treatments caused a leaching of the framework aluminum, which caused an increase in the particle agglomeration and a consequent decrease in the surface area. The leaching of the framework aluminum was also responsible for the increase of the isoelectric point and the decrease of the negative zeta potential.

Additionally, the mechanical treatment induces structural defects, such as breakup of the particles, which favored the dehydroxylation and the increase of the isoelectric point of the montmorillonites.



## Acknowledgments

We would like to thank the ANPCyT (project 1360/2006), the DGICYT and FEDER funds (project no. CTQ2010-14874) for financial support. The authors also wish to thank L. Garaventa (Segemar) for the SN2 data measurements.

## Appendix A. Supplementary data

Supplementary data associated with this article can be found, in the online version, at <http://dx.doi.org/10.1016/j.colsurfa.2013.01.040>.

## References

- [1] R.E. Grim, *Clay Mineralogy*, 2nd ed, McGraw-Hill, New York, 1968.
- [2] L. Fowden, R.M. Barrer, P.B. Tinker, Their structure, behaviour and use, in: *Clay Minerals*, The Royal Society, London, 1984, pp. 212–240.
- [3] K. Jasmund, G. Lagaly, in: *Tonminerale und Tone*, Steinkopf Verlag, Darmstadt, 1993.
- [4] S. Abend, N. Bonnke, U. Gutschner, G. Lagaly, Stabilization of emulsions by heterocoagulation of clay minerals and layered double hydroxides, *Colloids Polym. Sci.* 276 (1998) 730–737.
- [5] R.M. Torres Sánchez, Mechanochemical effects on physicochemical parameters of homoionic smectite, *Colloids Surf. A* 127 (1997) 135–140.
- [6] R.M. Torres Sánchez, C. Volzone, E.M. Curt, PZC determination of monoionic montmorillonite by transport number method, *Z. Pfla. Boden.* 155 (1992) 77–80.
- [7] K. Emmerich, Spontaneous rehydroxylation of dehydroxylates cis-vacant montmorillonite, *Clay Clay Miner.* 48 (2000) 405–408.
- [8] M. Chorom, P. Rengasamy, Effect of heating on swelling and dispersion of different cationic forms of smectite, *Clay Clay Miner.* 44 (1996) 783–790.
- [9] S. García-García, S. Wold, M. Jonsson, Effects of temperature on the stability of colloidal montmorillonite particles at different pH and ionic strength, *Appl. Clay Sci.* 43 (2009) 21–25.
- [10] S. Zhu, H. Hou, Y. Xue, Kinetic and isothermal studies of lead ion adsorption onto bentonite, *Appl. Clay Sci.* 40 (2008) 171–178.
- [11] N. Hargvey, W. Chantawong, Adsorption of heavy metals by ballclays, *J. Tokyo Univ. Inform. Sci.* 8 (2001) 79–87.
- [12] M. Epstein, S. Yariv, Visible-spectroscopy study of the adsorption of alizarinate by Al-montmorillonite in aqueous suspensions and in solid state, *J. Colloids Interface Sci.* 263 (2003) 377–385.
- [13] A. Tahani, M. Karroua, H. Van Damme, P. Levitz, Adsorption of a cationic surfactant on Na-montmorillonite: inspection of adsorption layer by X-ray and fluorescence spectroscopies, *J. Colloids Interface Sci.* 216 (1999) 242–249.
- [14] G. Chen, J. Pan, B. Han, H. Yan, Adsorption of methylene blue on montmorillonite, *J. Disp. Sci. Technol.* 20 (1999) 1179–1187.
- [15] G. Rytwo, S. Nir, L. Margulies, Adsorption interactions of diquat and paraquat with montmorillonite, *Soil Sci. Soc. Am. J.* 60 (1996) 601–610.
- [16] G. Sheng, C. Johnston, B. Teppern, S. Boyd, Adsorption of dinitrophenol herbicides from water by montmorillonite, *Clay Clay Miner.* 50 (2002) 25–34.
- [17] A.P. Magnoli, L. Tallone, C. Rosa, A.M. Dalcero, S.M. Chiacchiera, R.M. Torres Sánchez, Commercial bentonites as detoxifier of broiler feed contaminated with aflatoxin, *Appl. Clay Sci.* 40 (2008) 63–71.
- [18] M.G. Tenorio Arvide, I. Mulder, A.L. Barrientos Velazquez, J.B. Dixon, Smectite clay adsorption of aflatoxin vs. octahedral composition as indicated by FTIR, *Clay Clay Miner.* 56 (2008) 571–578.
- [19] I. Mulder, A.L. Barrientos Velazquez, M.G. Tenorio Arvide, N.G. White, J.B. Dixon, Smectite clay sequestration of aflatoxin B1: particle size and morphology, *Clay Clay Miner.* 56 (2008) 558–570.
- [20] J. Kulbicki, High temperature phases in montmorillonite, *Clay Clay Miner.* 5 (1958) 144–158.
- [21] H. Seyama, M. Soma, X-ray photoelectron spectroscopic study of the effect of heating on montmorillonite containing Na and K cations, *Clay Clay Miner.* 34 (1986) 672–676.
- [22] A. Weiss, G. Koch, Über einen Zusammenhang zwischen dem Verlust des innerkristallinen quellungsvermögens beim Erhitzen und dem Schichtaufbau bei glimmerartigen Schichtsilikaten, *Zeit Naturfor.* 16 (1961) 68–69.
- [23] N.K. Mitra, B. Sandilya, Flocculation characteristics of bentonite clay when substituted by different cations in exchangeable position, *Indian Ceram.* 13 (1969) 171–173.
- [24] V. Ramaswamy, S. Malwadkar, S. Chilukuri, Cu–Ce mixed oxides supported on Al-pillared clay: effect of method of preparation on catalytic activity in the preferential oxidation of carbon monoxide, *Appl. Catal. B: Environ.* 84 (2008) 21–29.
- [25] L.A. Galeano, A. Gil, M.A. Vicente, Effect of the atomic active metal ratio in Al/Fe-, Al/Cu- and Al/(Fe–Cu)-intercalating solutions on the physicochemical properties and catalytic activity of pillared clays in the CWPO of methyl orange, *Appl. Catal. Environ. B* 100 (2010) 271–282.
- [26] B. Vijayakumar, N. Mahadevaiah, G. Nagendrappa, B.S. Jai Prakash, Esterification of stearic acid with p-cresol over modified Indian bentonite clay catalysts, *J. Porous Mater.* 19 (2012) 201–210.
- [27] C.B. Molina, L. Calvo, M.A. Gilarranz, J.A. Casas, J.J. Rodriguez, Pd–Al pillared clays as catalysts for the hydrodechlorination of 4-chlorophenol in aqueous phase, *J. Hazard. Mater.* 172 (2009) 214–223.
- [28] M.N. Timofeeva, V.N. Panchenko, A. Gil, Y.A. Chesalova, T.P. Sorokina, V.A. Likholobov, Synthesis of propylene glycol methyl ether from methanol and propylene oxide over alumina-pillared clays, *Appl. Catal. B: Environ.* 102 (2011) 433–440.
- [29] S. Jagota, M.A. Harmer, M.E. Lemon, A. Jagota, E. McCarron, Pillared smectite clay coatings for ceramic–matrix composites, *J. Am. Ceram. Soc.* 78 (1995) 2243–2247.
- [30] C. Volzone, R.M. Torres Sánchez, Thermal and mechanical effects on natural and activated smectite structure, *Colloids Surf. A* 81 (1993) 211–216.
- [31] E.C. Ormerod, A.C. Newman, Water sorption on Ca-saturated clays: 2. Internal and external surfaces of montmorillonite, *Clay Miner.* 18 (1983) 289–299.
- [32] E. Ferrage, B. Lanson, B.A. Sakharov, V.A. Drits, Investigation of smectite hydration properties by modeling experimental X-ray diffraction patterns: Part I. Montmorillonite hydration properties, *Am. Miner.* 90 (8–9) (2005) 1358–1374.
- [33] M. Tschapek, R.M. Torres Sánchez, C. Wasowski, Handy methods for determining the isoelectric point of soils, *Z. Pfla. Boden* 152 (1989) 73–76.
- [34] E. Basaldella, R.M. Torres Sánchez, S. Pérez, D. Caputo, C. Colella, in: M.M.J. Treacy, B.K. Marcus, M.E. Bisher, J.B. Higgins (Eds.), *Proceeding of the 12th International Zeolites Conference, Vol. 3 Zeolite Synthesis from Clays: Effect of Impact Grinding on Kaolinite Structure and Reactivity*, Mater. Res. Soc, New York, 1999, pp. 1663–1670.
- [35] R.M. Torres Sánchez, E.I. Basaldella, J.F. Marco, The effect of thermal and mechanical treatments on kaolinite: characterization by XPS and IEP measurements, *J. Colloids Interface Sci.* 215 (1999) 339–344.
- [36] R.M. Torres Sánchez, S. Falasca, Specific surface and surface charges of some Argentinian soils, *Z. Pfla. Boden* 160 (1997) 223–226.
- [37] D. Siguin, S. Ferreira, L. Froufe, F. Garcia, Smectites, the relationship between their properties and isomorphic substitution, *J. Mater. Sci.* 29 (1994) 4379–4384.
- [38] H.-J. Sun, T.-J. Peng, Y. Liu, Calculation of crystal chemical formula of montmorillonite and classification, *J. Synth. Cryst.* 37 (2) (2008) 350–355.
- [39] L.J. Michot, F. Villieras, Developments in clay science, surface area and porosity, in: F. Bergaya, B.K. Theng, G. Lagaly (Eds.), *Handbook of Clay Sci.*, Elsevier, Amsterdam, 2006, pp. 965–978.
- [40] D.A. Laird, Layer charge influences on the hydration of expandable 2:1 phyllosilicates, *Clay Clay Miner.* 47 (1999) 630–636.
- [41] B. Caglar, B. Afsin, A. Tabak, E. Eren, Characterization of the cation-exchanged bentonites by XRPD, ATR, DTA/TG analyses and BET measurement, *Chem. Eng. J.* 149 (2009) 242–248.
- [42] G. Chen, B. Han, Y. Haike, Interaction of cationic surfactants with iron and sodium montmorillonite suspensions, *J. Colloids Interface Sci.* 201 (1998) 158–163.
- [43] R.M. Torres Sánchez, M. Genet, E. Gaigneaux, M. dos Santos Afonso, S. Yunes, Benzimidazole adsorption on external and interlayer surfaces of raw and treated montmorillonite, *Appl. Clay Sci.* 53 (2011) 366–373.
- [44] E. Bojemueller, A. Nennemann, G. Lagaly, Enhanced pesticide adsorption by thermally modified bentonites, *Appl. Clay Sci.* 18 (2001) 277–284.
- [45] I. Sondi, J. Bišćan, V. Pravič, Electrokinetics of pure clay minerals revisited, *J. Colloids Interface Sci.* 178 (1996) 514–522.
- [46] S. Lantenois, Y. Nedellec, B. Prélot, J. Zajac, F. Muller, J.-M. Duouillard, Thermodynamic assessment of the variation of the surface areas of two synthetic swelling clays during adsorption of water, *J. Colloids Interface Sci.* 316 (2007) 1003–1011.
- [47] F. Salles, J.M. Duouillard, R. Denoyel, O. Bildstein, M. Jullien, I. Beurroies, H. Van Damme, Hydration sequence of swelling clays: evolutions of specific surface area and hydration energy, *J. Colloids Interface Sci.* 333 (2009) 510–522.
- [48] X.-D. Liu, C. Xu, A. Lu, A thermodynamic understanding of clay-swelling inhibition by potassium ions, *Angew. Chem.* 38 (2006) 6300–6303.
- [49] P. Mignon, P. Ugliengo, M. Sodupe, E.R. Hernandez, Ab initio molecular dynamics study of the hydration of Li<sup>+</sup>, Na<sup>+</sup> and K<sup>+</sup> in a montmorillonite model. Influence of isomorphic substitution, *Phys. Chem. Chem. Phys.* 12 (2010) 688–697.
- [50] D.R. Collins, A.N. Fitch, C.R.A. Catlow, Dehydration of vermiculites and montmorillonites: a time-resolved powder neutron diffraction study, *J. Mater. Chem.* 2 (1992) 865–873.
- [51] H.-J. Nam, T. Ebina, F. Mizukami, Formability and properties of self-standing clay film by montmorillonite with different interlayer cations, *Colloids Surf. A* 346 (2009) 158–163.
- [52] G. Montes-Ha, J. Duplay, L. Martinez, Y. Geraud, B. Rousset-Tournier, Influence of interlayer cations on the water sorption and swelling – shrinkage of MX80 bentonite, *Appl. Clay Sci.* 23 (2003) 309–321.
- [53] Y. Zheng, A. Zaoui, I. Shahrou, Evolution of the interlayer space of hydrated montmorillonite as a function of temperature, *Am. Miner.* 95 (2010) 1493–1499.
- [54] G.E. Christidis, F. Dellisanti, G. Valdre, P. Makri, Structural modifications of smectites mechanically deformed under controlled conditions, *Clay Miner.* 40 (4) (2005) 511–522.
- [55] V.A. Drits, G. Besson, F. Muller, An improved model for structural transformations of heat treated aluminous dioctahedral 2:1 layer silicates, *Clays Clay Miner.* 43 (6) (1995) 718–731.

- [56] T. Missana, A. Adell, On the applicability of DLVO theory to the prediction of clay colloids stability, *J. Colloids Interface Sci.* 230 (2000), 150.
- [57] F. Thomas, L.J. Michot, D. Vantelon, E. Montarges, B. Prelot, M.J. Cruchaudet, F. Delon, *Colloids Surf. A* 159 (1999) 351.
- [58] J.D.G. Durán, M.M. Ramos-Tejada, F.J. Arroyo, F. González-Caballero, Rheological and electrokinetic properties of Na-montmorillonite suspensions, *J. Colloids Interface Sci.* 229 (2000) 107–117.
- [59] B. Lombardi, R.M. Torres Sánchez, P. Eloy, M. Genet, Interaction of thiabendazole and benzimidazole with montmorillonite, *Appl. Clay Sci.* 33 (2006) 59–65.
- [60] A. Delgado, F. Gonzalez-Caballero, J.M. Bruque, On the zeta potential and surface charge density of montmorillonite in aqueous electrolyte solutions, *J. Colloids Interface Sci.* 113 (1986) 203–211.
- [61] R.A. Kinsey, R.J. Kirkpatrick, J. Hower, K.A. Smith, E. Oldfield, High-resolution solid-state  $\text{Na}^{23}$ ,  $\text{Al}^{27}$ , and  $\text{Si}^{29}$  nuclear magnetic-resonance spectroscopic reconnaissance of alkali and plagioclase feldspars, *Am. Miner.* 70 (1985) 537–548.
- [62] G.E. Roch, M.E. Smith, S.R. Drachman, Solid state NMR characterization of the thermal transformation of an illite-rich clay, *Clay Clay Miner.* 46 (1998) 694–704.
- [63] J. Sanz, J.M. Serratos,  $^{29}\text{Si}$  and  $^{27}\text{Al}$  high-resolution MAS-NMR spectra of phyllosilicates, *J. Am. Chem. Soc.* 106 (1984) 4790–4793.
- [64] S.R. Drachman, G.E. Roch, M.E. Smith, Solid state NMR characterization of the thermal transformation of Fuller's earth, *Sol. State Nucl. Magn. Reson.* 9 (1997) 257–267.
- [65] C.A. Weiss, S.P. Altaner, R.J. Kirkpatrick, High-resolution Si-29 NMR-spectroscopy of 2-1 layer silicates-correlations among chemical-shift, structural distortions, and chemical variations, *Am. Miner.* 72 (1987) 935–942.
- [66] D. Mueller, D. Hoebbel, W. Gessner,  $\text{Al}^{27}$  NMR-studies of aluminosilicate solutions-Influences of the 2nd coordination sphere on the shielding of aluminum, *Chem. Phys. Lett.* 84 (1981) 25–29.
- [67] G. Engelhardt, D. Michel, in: *High-Resolution Solid State NMR of Silicates and Zeolites*, Wiley, New York, 1987.
- [68] A.D. Irwin, J.S. Holmgren, J. Jonas,  $\text{Al}^{27}$  and  $\text{Si}^{29}$  NMR-study of sol-gel derived aluminosilicates and sodium aluminosilicates, *J. Mater. Sci.* 23 (1988) 2908–2912.
- [69] P.J. Chupas, C.P. Grey, Surface modification of fluorinated aluminas: application of solid state NMR spectroscopy to the study of acidity and surface structure, *J. Catal.* 224 (2004) 69–79.
- [70] I. Dékány, L. Turi, A. Fonseca, J.B. Nagy, The structure of acid treated sepiolites: small-angle X-ray scattering and multi MAS-NMR investigations, *Appl. Clay Sci.* 14 (1999) 141–160.